Research Article

pH-sensitive biopolymeric hydrogel-based on indole-3-acetic acid for wound healing and anti-cancer applications

G. Chitra[1] · M. S. Selvi[2] · D. S. Franklin[3] · S. Sudarsan[3] · M. Sakthivel[4] · S. Guhanathan[2]

Abstract
Gold nanoparticles (AuNPs) are widely used and important nanomaterials and combine with hydrogels to design novel nanocomposite hydrogels. An emerging approach to strengthen the polymeric hydrogels and to include multiple functionalities focuses on incorporating nanoparticles within the hydrogel network. This present investigation focused on the most recent developments in the field of nanocomposite hydrogels with emphasis on biomedical applications. The pH-responsive nanocomposite hydrogels based on indole-3-acetic acid (IAA), which has extracted from leaf of *Stachytarpheta jamaicensis,* citric acid, diethylene glycol and colloidal gold nanoparticles. The obtained nanocomposite hydrogels found to have desired surface morphology and enhanced pH-sensitive swelling and thermal stability. The resultant nanocomposite hydrogels may be recommended for biomedical applications mere in future such as pH-sensitive drug delivery, wound healing application, anti cancer, antimicrobial material, antioxidant, cytotoxicity with more than 80% cell viability and nanomedicine.

Keywords Stachytarpheta jamaicensis · Indole-3-acetic acid · Antimicrobial · Antioxidant · Cytotoxicity · Wound healing · Anti-cancer

1 Introduction

Hydrogels are three-dimensional networks of hydrophilic polymers with a porous structure, which are insoluble in water but can absorb and retain a large amount of water or biological fluids inside the porous network [1]. Hydrogels have a "soft and wet" character just like biological material with high water content absorbing property. Bulk gold is the most precious metals and considered as inert at microscopic level [2], which has impressed researchers due to different improved characteristics e.g., plasmon-related fields.

The AuNPs are exhibited for various applications like molecular imaging [3], surfaces improved raman scattering [4, 5], catalytic activity [6], diagnostics [7], antimicrobial activity [8] and antifungal activity [9] and treatment of rheumatoid arthritis [10, 11]. When discussing with metal nanoparticles on their interaction with eukaryotic cells and their appropriate toxicological applications [12]. The nanoscale range of hydrogels shows non-toxicity when compared to bulk size materials [13–16]. Smaller size (< 20 nm) of AuNPs is great interest for research of their cytotoxicity properties in pharmacology, food, medicine, and water purification. The expanding of the research field when the interaction of metal nanoparticles with

✉ S. Guhanathan, sai_gugan@yahoo.com; G. Chitra, chitramuralikrishnan@gmail.com; M. S. Selvi, msselvi1984@gmail.com; D. S. Franklin, loyolafrank@yahoo.co.in; S. Sudarsan, srsudarsan29@gmail.com; M. Sakthivel, msakthi81986@gmail.com | [1]Department of Chemistry, Bangalore College of Engineering and Technology, Chandapura, Bangalore 560099, India. [2]PG & Research Department of Chemistry, Muthurangam Government Arts College, Vellore, Tamilnadu 632002, India. [3]Department of Chemistry, C. Abdul Hakeem College of Engineering and Technology, Melvisharam, Tamilnadu 632509, India. [4]Department of Chemistry, Bharathiar University, Coimbatore 641046, India.

microorganisms such as fungus and viruses e.g. HIV [17]. In general, the hydrogel or gold nanocomposites showed advanced antimicrobial activity, there is an urgent requirement for new and improved approaches for bacterial destruction.

The smaller size and the hefty surface to volume proportion, metal nanoparticles have been receiving much concentration in recent times towards different applications, extraordinarily in the area of nano-biotechnology [18–20]. However, the different natural biopolymers like elastin, collagen, and gelatin are interesting materials for hydrogel developments. To improve their bioactivity in wound care applications, a number of researchers introduced inorganic metals [21]. Antioxidant property at high concentrations, reactive oxygen species (ROS) can encourage harsh tissue damage and even lead to neoplastic transformation and declining the healing process by damages in cellular membranes, DNA, proteins, and lipids [22, 23]. Antioxidants reduce these adverse effects of wounds by removing products of inflammation. They contradict the excess proteases and ROS often produced by neutrophil accumulation at the injured site and safeguard protease inhibitors from oxidative damage [24]. The most likely mechanism of antioxidant protection is the direct interaction of the extracts compounds and the hydrogen peroxide rather than altering the cell membranes and limiting damage [25]. Compounds with high radical-scavenging capability have been shown to ease wound-healing.

In general, indole derivatives are biologically significant compounds with a broad range of therapeutic properties. Antibacterial [26], Antifungal [27] and Antioxidant properties [28, 29] have been reported to be connected with the indole-based nucleus. Indolic compounds are competent antioxidants, protecting both lipids and proteins from peroxidation, and it is identified that the indole structure controls the antioxidant efficacy in biological systems [30]. Generally, the high antioxidant activity of hydrogel leads to low cytotoxicity. Hence, the pro-oxidant result of the electron retreating nitrogen group in the matrix [31].

The scope of this work for various industrial and biomedical applications, there is a continuous demand for improved the polymers and their nanocomposites, which possess pH sensitivity, antibacterial, and antifungal as well as antioxidant properties at reduced costs. Such requirements form a combination of properties difficult to attain with existing materials. Hence, to meet the end use applications, synergetically combined materials like biopolymeric materials and nanomaterials having a maximum number of applications are mandatory. So, the present investigation was centered on accomplishing with indole-3-acetic acid based citric acid and diethylene glycol along with gold nanoparticles. Indole-3-acetic acid has been extracted from leaves of *Stachytarpheta jamaicensis*.

The AuNPs introduced in hydrogel network by in situ reductions of $HAuCl_4$ by using trisodium citrate as a reducing agent. The gold nanoparticle was characterized by using TEM and UV analysis. The synthesized gold nanoparticle was mixed with hydrogel network formed NCHs (G_1ICD, G_2ICD). The hydrogel (ICD) and NCHs were fully characterized by using UV, FT-IR, TGA, TEM, and SEM–EDX. Swelling equilibrium was calculated at various buffer solutions (3–10) results shown better swelling equilibrium in acidic media and applied for wound healing and anticancer activity.

2 Experimental

2.1 Materials and methods

Anhydrous citric acid (CA), diethylene glycol (DEG) tetrachloroauric acid ($HAuCl_4$) and trisodium citrate were purchased from Merck (India).

### 2.2 Preparation of indole-3-acetic acid

Stachytarpheta jamaicensis leaves were collected and dried in the room temperature. Then dried leaves powdered and extracted using soxhlet apparatus around 70 h at 60 ℃. The aqueous solution was subjected to concentrate using rotary flash evaporator at 40 ℃ under reduced pressure then the sample was dried in hot air oven at 50–60 °C, the dried crude indole-3-acetic acid was collected.

2.3 Preparation of gold nanoparticles by citrate reduction of $HAuCl_4$

The Gold nanoparticle was prepared by the Turkevich et al. Method [32]. Chloroauric acid ($HAuCl_4$) was boiled with vigorous stirring at 95 °C and followed by rapid addition of trisodium citrate, which act as reducing agent. The pale yellow color turned to wine red followed by stirring for 30 min. The colloidal AuNps solution was stored at room temperature in a dark brown bottle.

2.4 Preparation of Au nanocomposite hydrogel

Previously, our research group have reported the synthesis of hydrogel (ICD) based on indole-3-acetic acid in two steps [33]. In brief, esterification was carried out from citric acid and diethylene glycol in the nitrogen atmosphere at 160 °C. Further, indole-3-acetic acid was added and formed sticky compound. During the formation of the transparent gel, gold nanoparticle was added. The entire mixture was vigorously stirred for 30 min and continues the reaction for 3 h. The formation of brown glassy gels
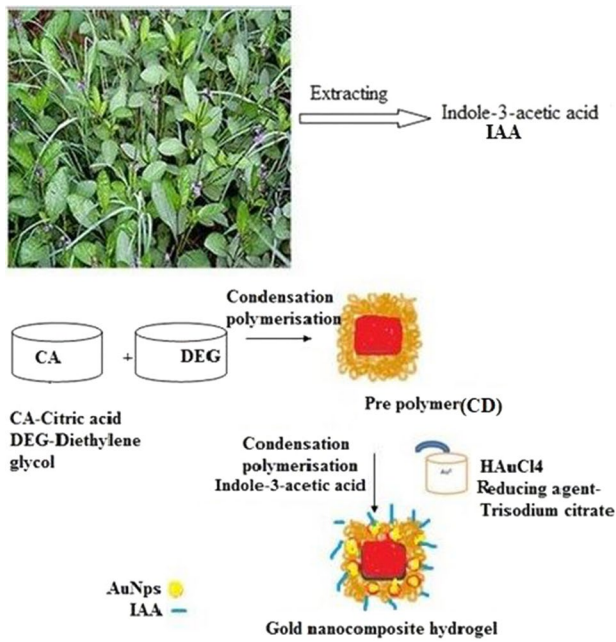
Scheme 1 Schematic representation of gold nanocomposite hydrogels

Table 1 Feed composition of polymeric hydrogel and nanocomposite hydrogels

S. no	Sample	Composition (mol)			AuNps
		CA	DEG	IAA	
1	ICD	0.025	0.025	0.025	–
2	G_1ICD	0.025	0.025	0.025	2 ml
3	G_2ICD	0.025	0.025	0.025	5 ml

infers the formation of nanocomposite hydrogel (NCH) of polymerization.

Finally, the resulted NCHs were immersed in distilled water for 2 days then removed unreacted monomer and dried the NCHs in an oven. The complete schematic representation and description of hydrogels were presented in Scheme 1 and Table 1 respectively.

2.5 Characterization of gold NCHs

Indole-3-acetic acid has extracted from leaves of *Stachytarpheta jamaicensis* and confirmed by ^{1}H NMR, ^{13}C-NMR and HPLC analysis. The structure of hydrogel was recorded using FT-IR (Shimadzu-8400S) spectrophotometer. The gold nanoparticles into the hydrogel matrix were established by the absorption of HITACHI U-2900 UV–visible spectrophotometer in the range of 300-700 nm. Scanning Electron Microscopy (SEM) images were taken using Hitachi SU6600. Field Emission Scanning Electron

Microscope (FESEM) and Energy-dispersive X-ray (EDX) spectroscopy analysis are used to confirm the incorporation of gold in nanocomposite hydrogels. Transmission electron microscopy (TEM) used in the model of this instrument has JEM 2000. Resolution is Point: 0.23 nm, Lattice: 0.14 nm then voltage is 200 kV and the magnification occurs 2000×–1,500,000×.

2.6 Swelling equilibrium studies

Swelling equilibrium experiment was examined in phosphate buffer solutions (PBS) of various pH ranging from 3.0 to 10.0. Swollen gels were removed from the buffer solution after 48 h and then weighed and placed in the same bath. The pH values were precisely checked with a pH meter and the equilibrium swelling was calculated in Eq. 1.

$$S_{eq}\% = \frac{W_{eq} - W_d}{W_d} \times 100 \qquad (1)$$

where W_d and W_{eq} are the weights of the sample before swollen after swollen at equilibrium, respectively.

2.7 Antibacterial activity

Different concentrations of Samples were used in this study. Nutrient Agar (NA) plates were inoculated with test organisms. The plates were evenly spread out. Then wells were prepared in the plates with a cork borer. Each well was loaded with 0.1 ml of a corresponding concentration of the sample and 10 μg of gentamycin dissolved in 1 ml of DMSO was used as a positive control for antibacterial activity. The plates were incubated for 24 h at 37 °C. The development of the inhibition zone was measured and recorded.

2.8 Antifungal activity

Different concentrations of Samples (1.25/2.5/5 mg/100 μl/well) were used in this study. Muller hinton agar (MHA) plates were inoculated with test organisms. The plates were evenly spread out. Then wells were prepared in the plates with a cork borer. Each well was loaded with 0.1 ml of the corresponding concentration of sample and *Fluconazole* was used as a positive control. The plates were incubated for 48 h at 37 °C. The development of the inhibition zone around the well was measured [33, 34].

2.9 Antioxidant activity

2.9.1 Case 1: free radical scavenging activity on DPPH

The ability of the extracts to annihilate the DPPH radical (1, 1-diphenyl-2-picrylhydrazyl) was investigated by the method described by Blois [35]. A stock solution of a compound was prepared to the concentration of 10 mg/ml. Different concentration of the extract (25, 50, 75, 100, 200 and 250 μg) of the sample was added, at an equal volume to a methanolic solution of DPPH (0.1 mM). The reaction mixture is incubated for 30 min at room temperature; the absorbance was recorded at 517 nm. The experiment was repeated for three times and ascorbic acid was used as the standard control.

The annihilation activity of free radicals was calculated in % inhibition according to the following formula

$$\% \text{ of Inhibition} = (A \text{ of control} - A \text{ of Test} / A \text{ of control}) \times 100$$

The analysis was performed in triplicate. The sample concentration providing 50% inhibition (IC_{50}) under the assay condition was calculated from the graph of inhibition percentage against sample concentration.

2.9.2 Case 2: nitric oxide radical scavenging activity

The nitric oxide assay was performed as described previously with slight modification. Sodium nitroprusside (1.5 mL, 10 mM) in Phosphate buffered saline was mixed with the samples of concentrations–250, 500 and 1000 μg. The amount of nitrite, a stable metabolite of NO, was measured using Griess reagent (1% sulfanilamide and 0.1% naphthyl ethylenediamine dihydrochloride in 2.5% phosphoric acid). The sample with sodium nitroprusside was mixed with 1.5 ml of Griess reagent. Subsequently, the mixture was incubated at room temperature for 10 min and the absorbance at 540 nm was measured in a UV spectrophotometer.

The annihilation activity of free radicals was calculated in % inhibition according to the following relation:

$$\% \text{ of Inhibition} = (A \text{ of control} - A \text{ of Test} / A \text{ of control}) \times 100$$

The analysis was performed in triplicate. The sample concentration providing 50% inhibition (IC_{50}) under the assay condition was calculated from the graph of inhibition percentage against sample concentration.

2.10 MTT assay–cytotoxicity

The relative cytotoxicity of hydrogel was determined by an MTT viability assay developed for high throughput screening (HTS). The MTT substrate is prepared in a physiologically balanced solution, added to cells in culture, usually at a final concentration of 0.2–0.5 mg/ml, and incubated for 1–4 h.

The quantity of formazan (presumably directly proportional to the number of viable cells) was measured by recording changes in absorbance at 570 nm using a plate reading spectrophotometer. Viable cells with an active metabolism, which convert MTT into a purple colored formazan product. When cells die, they lose the ability to convert MTT into formazan and DMSO was added to dissolve formazan crystals. Untreated cells were taken as the control with 100% viability.

2.11 Scratch wound healing assay

Grow cells in Dulbecco's modified eagle's medium (DMEM) supplemented with 10% FBS Seed cells into 24-well tissue culture plate at a density that after 24 h of growth, they should reach ~ 70–80% confluence as a monolayer. Gently and slowly scratch the monolayer with a new 1 ml pipette tip across the center of the well. While scratching the surface of the well, the long-axial of the tip should always be perpendicular to the bottom of the well. The resulting gap distance, therefore, equals the outer diameter of the end of the tip. The gap distance can be adjusted by using different types of tips. Scratch a straight line in one direction. Scratch another straight line perpendicular to the first line to create a cross in each well.

After scratching, gently wash the well twice with medium to remove the detached cells. Replenish the well with fresh medium. Note: Medium may contain ingredients of interest that you want to test, e.g., chemicals that inhibit/promote cell motility and/or proliferation. Grow cells for an additional 48 h (or the time required if different cells are used). Wash the cells twice with 1 × PBS, then fix the cells with 3.7% paraformaldehyde for 30 min. Stain the fixed cells with 1% crystal violet in 2% ethanol for 30 min. Take photos for the stained monolayer on a microscope. Set the same configurations of the microscope when taking pictures for different views of the stained monolayer. The gap distance can be quantitatively evaluated using software such as photoshop or image. To reduce variability in results, it's suggested that multiple views of each well should be documented, and each experimental group should be repeated multiple times.

2.12 Anti-cancer application

Anti-Cancer activity carried out by using, A549, MDA-MB-231 and PC3 cancer cell lines after 24-h drug treatment by using crystal violet dye binding assay. To prepare cells and biopolymer compounds in 96-well plates containing a final volume of 100 μl/well. Further, incubate for the particular period of

Fig. 1 a ^{1}H NMR spectroscopy of IAA, **b** ^{13}C NMR spectroscopy of IAA
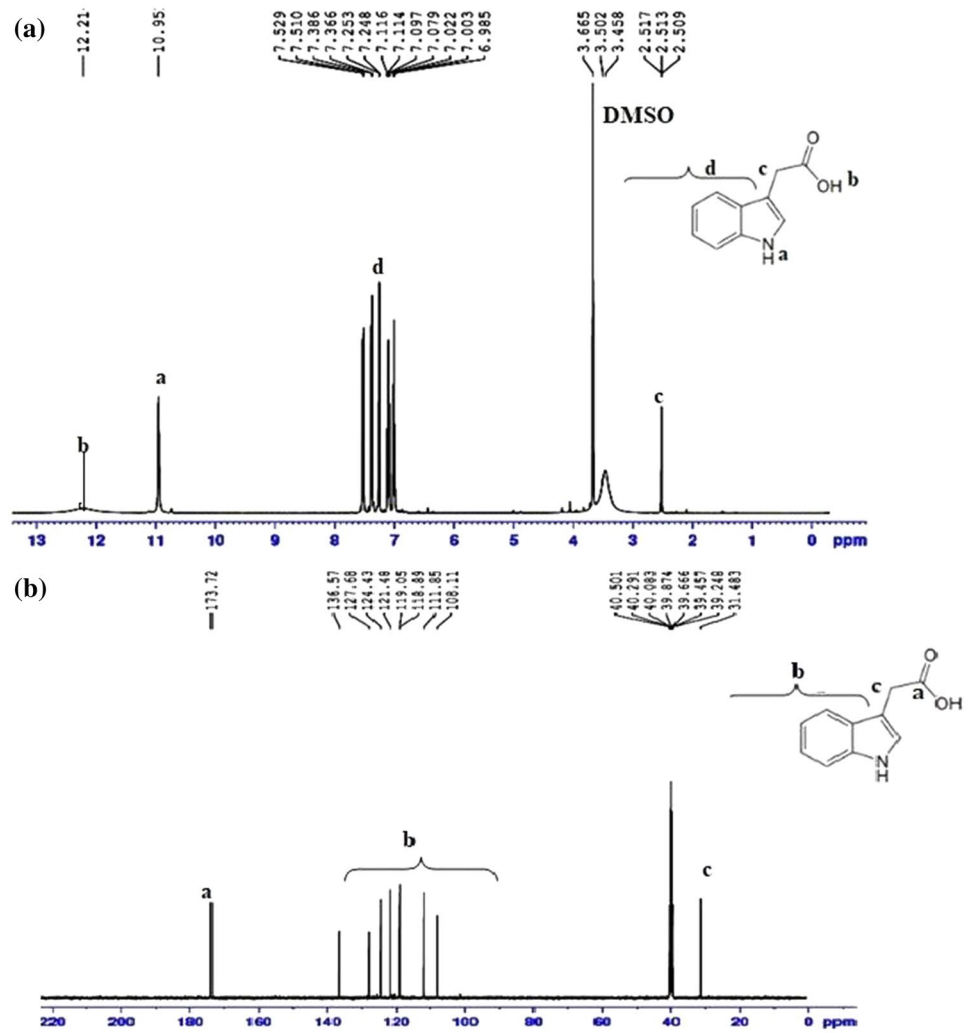
exposure and add 10 µl MTT solution per well to achieve a final concentration of 0.45 mg/ml. Then, incubate the solution for 1–4 h at 37 °C and add 100 µl solubilization solution to each well to dissolve formazan crystal and mix complete solubilization and the absorbance at 570 nm.

3 Results and discussion

3.1 ^{1}H NMR and ^{13}C NMR spectral studies of indole-3-acetic acid

Figure 1a represented ^{1}H NMR of IAA, peaks at 2.509–2.517 ppm relate to side chain –CH$_2$ proton and peak at 12.216 ppm contain side chain –COOH proton. The peaks of indole ring protons at 6.990–7.529 ppm and –NH proton from indole ring present at 10.951 ppm. ^{13}C NMR spectra of IAA (Fig. 1b) has discussed as follows, the peak at 31.49 ppm containing –CH$_2$ group attached in the third position of the indole ring. The multiple peaks of IAA was

observed at 108.11–136.57 ppm, the peak at 173.72 ppm confirms the third position of acid carbon in IAA [36]. Hence, the compound confirmed as indole-3-acetic acid from *Stachytarpheta jamaicensis* leaves.

3.2 HPLC analysis of indole-3-acetic acid

Typical chromatograms from the HPLC analysis of IAA in plant extracts are shown in Fig. 2. The SAX column gave good separations of IAA. One of the advantages of the HPLC method is that only milligram amounts of leaves powder is required. The indoles possess acidic (IAA) character and that the pH of the mobile phase is an important factor influencing the retention time and peak shape of ionizable compounds. The retention times were approximately 6 min, which has confirmed the presence of indole-3-acetic acid in leaves extract [37].
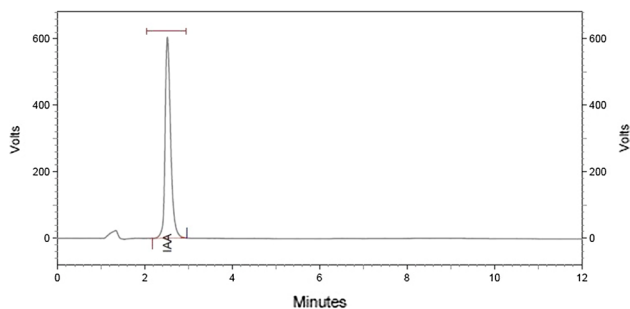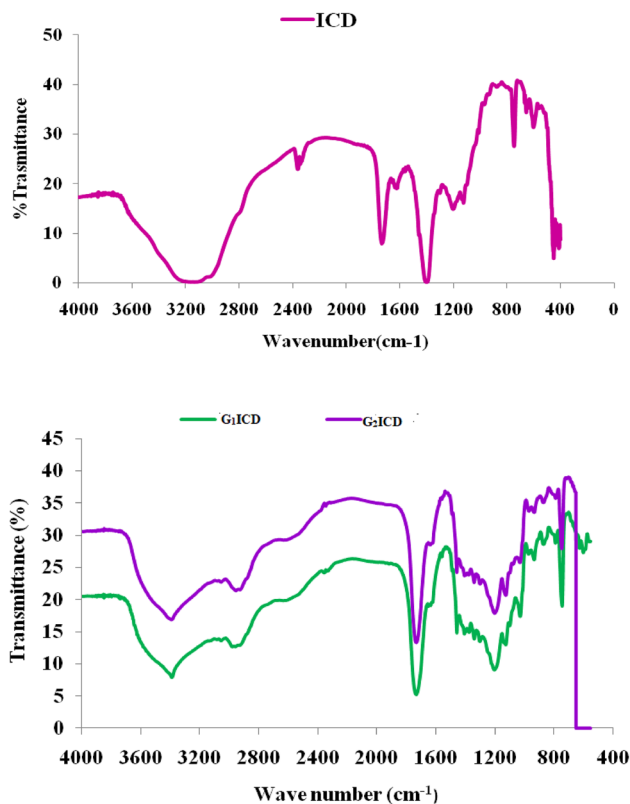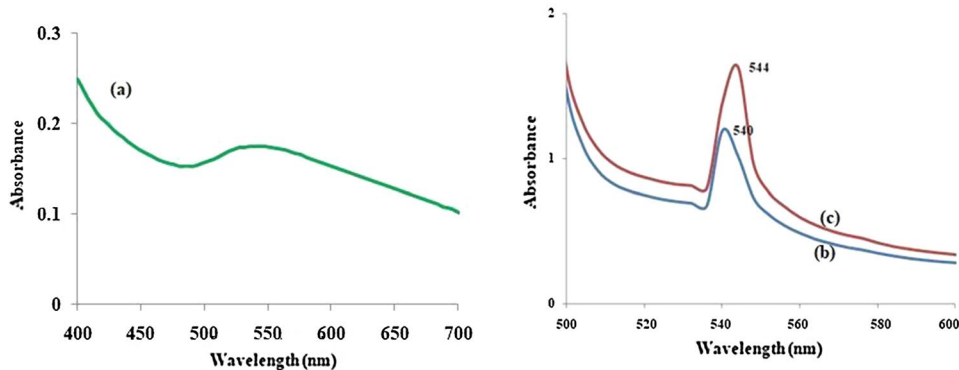
Fig. 2 HPLC analysis of IAA

Fig. 3 FT-IR spectroscopy of ICD, G_1ICD and G_2ICD

## 3.3 Fourier transform spectroscopy (FT-IR)

FTIR spectroscopy is a significant tool to confirm the interaction between metal and polymer. The FTIR spectra of pure hydrogel and their NCHs have shown in Fig. 3. ICD hydrogel has shown the characteristic –C=O stretching vibration of the ester group at 1725 cm^{-1} and a weak shoulder peaks at 2348 cm^{-1} related to the aliphatic –CH stretching frequency. The absorption band appeared at 1620 cm^{-1} attributed to –COO$^-$ stretching in the ICD hydrogel [38]. The peaks at 742 cm^{-1} were attributed –CH– out of plane bending of an aromatic ring. These results confirmed the incorporation of aromatic moieties presents in ICD.

The sharp peak at 3389 cm^{-1} can be attributed to either the hydrogen bonded –OH in diol and –NH bond or both (overlapped) [39]. For G_1ICD, the peak at –C=O stretching frequency of ester group was 1730 cm^{-1} and in G_2ICD peak contains at 1722 cm^{-1} respectively. The new distinguished peaks appeared at 548 cm^{-1} and 600 cm^{-1} for G_1ICD and G_2ICD respectively, which confirmed the successful incorporation of AuNPs in hydrogels [40]. It also evidenced from band appeared at 1456 cm^{-1} attributed to –COO$^-$ stretching for G_1ICD and 1487 cm^{-1} for G_2ICD with the addition of shifting some of the important peaks of –OH, –CH$_2$, and –NH towards the lower region. Several peaks were shortened and split up corroborated of co-ordination bond formed among AuNps and the electron-rich nitrogen atom of the heterocyclic compound in hydrogels. It causes intensification in bond length, ultimately lead to shifting of frequency which has confirmed the formation of the gold NCHs [41].

3.4 Ultra violet spectroscopy

Ultra violet spectroscopy analysis of AuNPs and NCHs were displayed in Fig. 4a. The absorption peak of AuNPs was indicated at 540 nm, which might be related to the surface plasmon resonance effect of AuNPs [42]. G_1ICD and

Fig. 4 UV absorption spectroscopy of **a** gold nanoparticle, **b** G_1ICD, **c** G_2ICD

Fig. 5 TEM Images of **a** G_1ICD, **b** G_2ICD
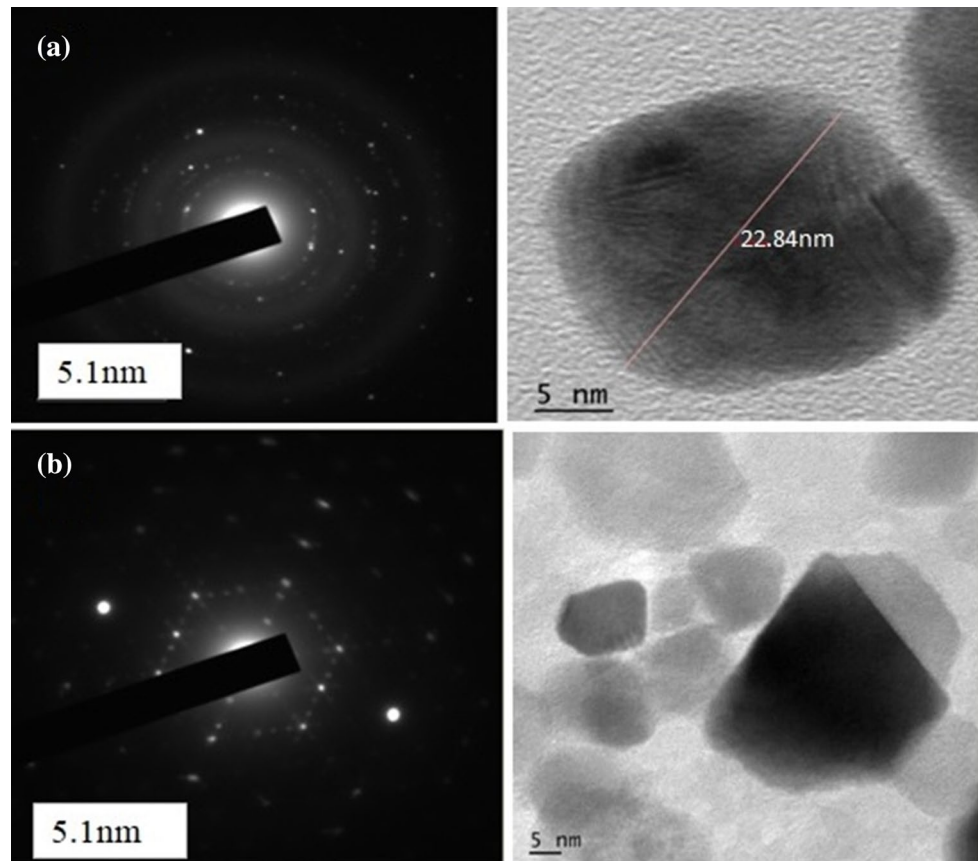
G_2ICD have shown an important peak at 540 and 544 nm (Fig. 4b, c).

As the concentration of HAuCl$_4$ solution increases, broadening the peak and redshift band with stronger strength was clearly observed in UV spectra, which might be due to the larger size of gold nanoparticles and increasing the absorbance. So, the absorption of G_1ICD and G_2ICD were 1.6 and 1.8 due to the variation of position, shape and particle size and further verified by TEM analysis. The shift towards longer wavelength with the increasing particle size of AuNPs is related to the differences in the frequency of surface plasmon oscillations of the free electrons [43, 44], which confirmed the successful incorporation of AuNPs in the hydrogel network.

### 3.5 High-resolution transmission electron microscopic analysis

Gold nanoparticles and NCHs exhibited a broad absorption band at 540 nm, which is consistent with the formation of spherical AuNPs [45] with the average size found to be 17 nm. The size of the gold nanoparticles in NCHs (G_1ICD and G_2ICD) was observed about 28 nm (Fig. 5a) and 57 nm (Fig. 5b). The shape and the size of AuNPs (low concentration) were spherical and smaller when increasing

the concentration of the AuNPs where some of the particles tends to change the nonspherical shape and increase in size. The size of the AuNPs decreased with increasing the biological activity due to the increasing surface activity of NCHs when compared with the larger size and nonspherical gold nanoparticles in NCHs [46, 47].

3.6 Field emission scanning electron microscopy-energy dispersive X-ray analysis (EDX)

FESEM-EDX analysis of G_1ICD and G_2ICD were illustrated in Fig. 6. The results showed the presence 0.14 wt% of Au, 1.52 wt% of oxygen, 56.31 wt% of carbon and 42.59 wt% of nitrogen for G_1ICD (Fig. 6a) and 0.25 wt% of Au, 2.17 wt% of oxygen, 56.13 wt% of carbon and 41.45 wt% of nitrogen for G_2ICD (Fig. 6b) respectively. An absorption peak has appeared at 2 keV, which has the characteristic of gold nanoparticles [48].

Both NCHs were found to have around 99% of surface composition which has indicated the high purity of the composite samples. FESEM of ICD hydrogel and NCHs have been displayed in Fig. 7. The ICD hydrogel shows a less porous and uneven and moon-like surface morphology,
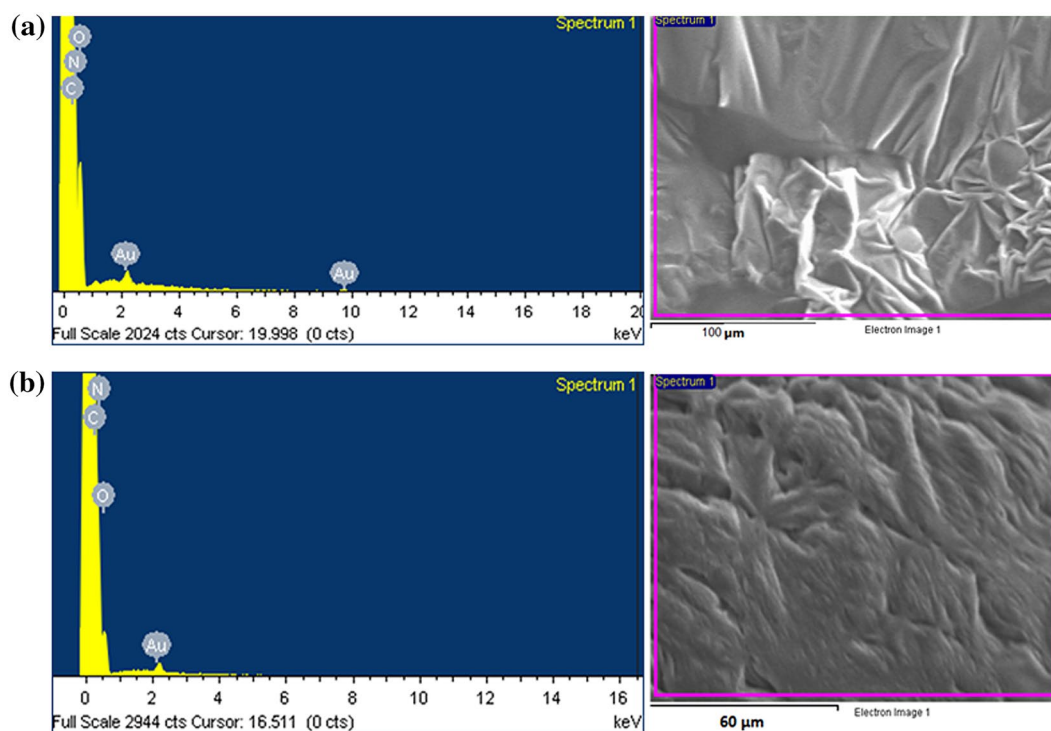
Fig. 6 EDAX Images of **a** G_1ICD, **b** G_2ICD

whereas G_1ICD found to have spherical in shape of gold nanoparticle marked in red color with complete dispersion in the polymer matrix but G_2ICD contains spherical and nonspherical shapes of gold nanoparticle (red mark) present in the polymer composite. The spherical shape of the nanoparticles has attributed to the biological property than other shapes of nanoparticles [49], so which has proved G_1ICD was best biological property than G_2ICD. SEM results were strongly supported by the swelling behavior of pure hydrogel and respective NCHs. The decrease of swelling with respect to the increasing content of AuNPs, which might be the alteration and a huge influence on the surface morphology of hydrogels.

3.7 Swelling equilibrium

The complete swelling profile was represented in Fig. 8. The hydrogel and NCHs were exhibited the equilibrium swelling higher at acidic pH than alkaline pH. Swelling equilibrium studies of ICD hydrogel was greater than NCHs due to dispersion of AuNPs resulted in high stiffening of the polymeric chains in NCHs [50]. Swelling equilibrium of ICD hydrogel increased in acidic media, this can be attributed due to the presence of polar groups (OH,-COOH) in the polymeric chain and the presence of ionic groups in polymeric chain results, increasing swelling equilibrium. Hence, the decline in osmotic pressure and electrostatic

repulsion among protonated amino groups (-NH) which leads to decreasing swelling in a basic medium [51]. The overall swelling performance of hydrogels and their composite as follows $ICD > G_1ICD > G_2ICD$. The basis of links between AgNP's and electron rich N atoms present in the polymeric chain which retained the water penetration ability of the NCHs and decreasing the swelling equilibrium [52].

Moreover, the swelling ability was changed after the formation of NCHs. Ma et al. [53] reported the formation of nanoparticles in hydrogel matrix improved the flexibility of hydrogel network, resulted in the likelihood of NCHs getting linked to the strong interactions between nanoparticles and hydrophilic groups present in the polymeric hydrogel matrix.

3.8 Thermal analysis

Figure 9 represents the thermal stability of gold nanocomposite hydrogel based on DEG, CA and IAA. In G_1ICD hydrogel has three stages of decomposition; the first stage was 180 and 240 °C with 25% loss of weight due to loss of water and breakdown side chain materials. Second stage decomposition was between 250 and 300 °C with 20% weight loss due to degradation of the side chain aromatic network. The third stage decomposition was mentioned in the range of 300–400 °C with 20% weight loss attributed to
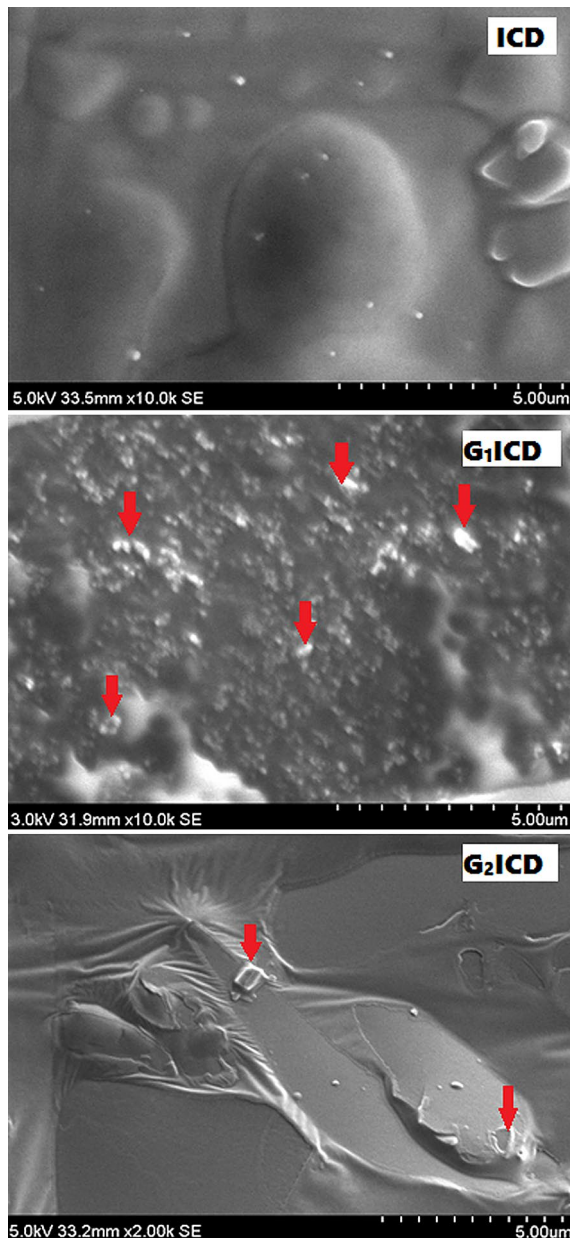
Fig. 7 SEM Images of **a** ICD, **b** G_1ICD, **c** G_2ICD

Fig. 8 Swelling equilibrium studies of **a** ICD, G_1ICD and G_2ICD
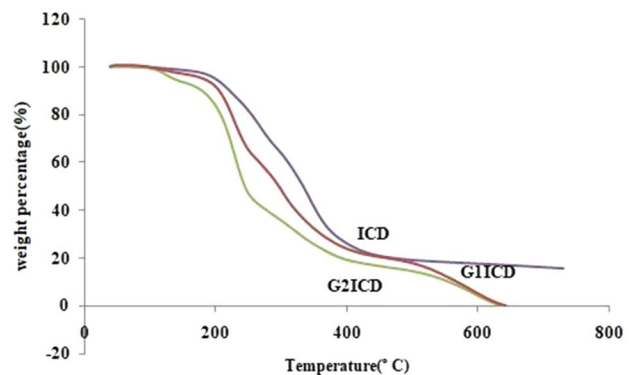
Fig. 9 Thermogravimetric analysis of ICD G_1ICD G_2ICD

carbonization and breakage of gold in hydrogel network. The G_2ICD hydrogel has shown in three-stages of decomposition. The first stage decomposition was detected between 130 and 160 °C with a weight loss of 5% due to loss of water.

The second stage decomposition was in the temperature range from 160 to 250 °C with a weight loss of 45% might be due to the breakdown of the ester bond, aromatic network and chain scission. The third stage decomposition was mentioned in the range of 250–390 °C with 25% weight loss attributed to carbonization and breakage of gold of the hydrogel network. G_1ICD was lower
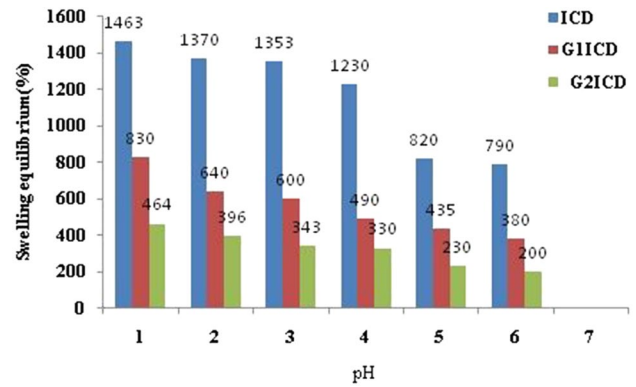
thermal stability than G_2ICD, due to the impact of chain length between gold nanoparticles and hydrogel network [54]. The thermal stability of NCHs was reduced when compared with pure hydrogel (ICD).

3.9 Biological applications

3.9.1 Antibacterial activity

Antibacterial studies have been noticed in view of G_1ICD and G_2ICD against two pathogens like *S. aureus* and *E. coli* using agar diffusion method with positive control *gentamicin* (10 µg/ml). Figure 4, 10 summarizes the antibacterial activity of G_1ICD and G_2ICD varied with concentrations like 500, 1000, 1500, 2000 µg/ml respectively. No microbial activity at 500 µg/ml of G_1ICD and 500 and 1000 µg/ml for G_2ICD against *S. aureus*. Upon increasing the strength of G_1ICD to 1000, 1500 and 2000 µg/ml, the inhibition zone (mm) has been varied viz., 8.33, 10.67 and 11.67 mm and percentage activity has been calculated 46, 59 and 65% compared with *gentamicin*. On the other hand, G_2ICD estimated the good inhibition to 1500 and 2000 µg/ml against *S. aureus*. Similarly, increasing the concentration

Fig. 10 Antibacterial activity of **a** G_1ICD, **b** G_2ICD
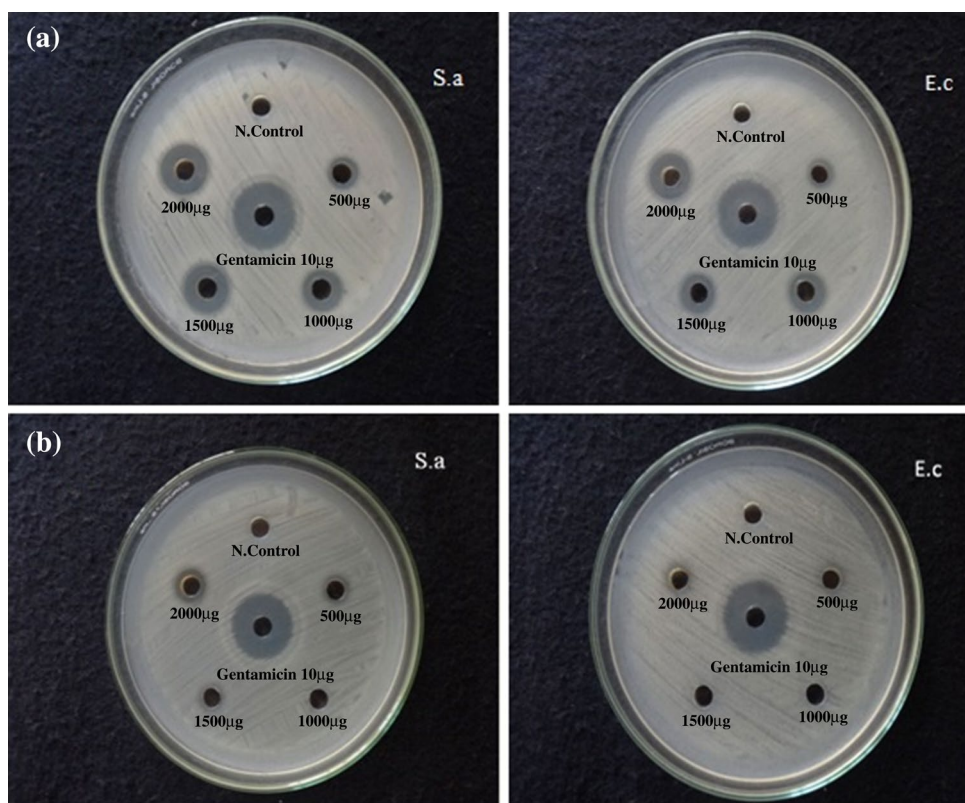
of both G_1ICD and G_2ICD, the inhibition activity increased to *E. coli*. Pure hydrogel ICD hydrogel shows no activity against three bacterial strains due to the presence of gold nanoparticles lead to enhance the antibacterial activity [55–57]. From G_1ICD and G_2ICD, the antibacterial activity of G_1ICD has excellent activity than G_2ICD could be a smaller size (17 nm) of nanoparticles evidenced from TEM images.

3.9.2 Antifungal activity

Figure 11a–c summarized the antifungal activity of ICD, G_1ICD and G_2ICD using well diffusion method with selected fungi such as *Aspergillus fumigatus* and *Candida albicans* at different concentration 500, 1000, 1500 and 2000 μg/ml and *Ketaconazole* have considered as standard. The zone of inhibition of ICD hydrogel *Aspergillus fumigatus* and *Candida albicans* was about 10.26 mm and 10.21 mm at 2000 μg/well. This result revealed that G_1ICD has no antifungal activity against *Candida albicans* at 500 μg/ml and G_2ICD has no activity against *Candida albicans* at 500, 1000 μg/ml.

By increasing the concentration to 1000, 1500 and 2000 μg/ml, the inhibition zone increased linearly such as 5.00, 6.27, and 9.67 mm for G_1ICD with respect to the standard. Similarly, G_2ICD found to have lesser inhibition

at 1500 μg/ml and good inhibition for 2000 μg/ml against *Candida albicans*. Similarly, the antifungal activity increases against *Aspergillus fumigatus* of both G_1ICD and G_2ICD by increasing the concentration from 500 to 2000 μg/ml. Based on the above results, G_1ICD was greater antifungal activity due to the smaller particle size of Au, larger surface area and respective monomers of hydrogel [58, 59].
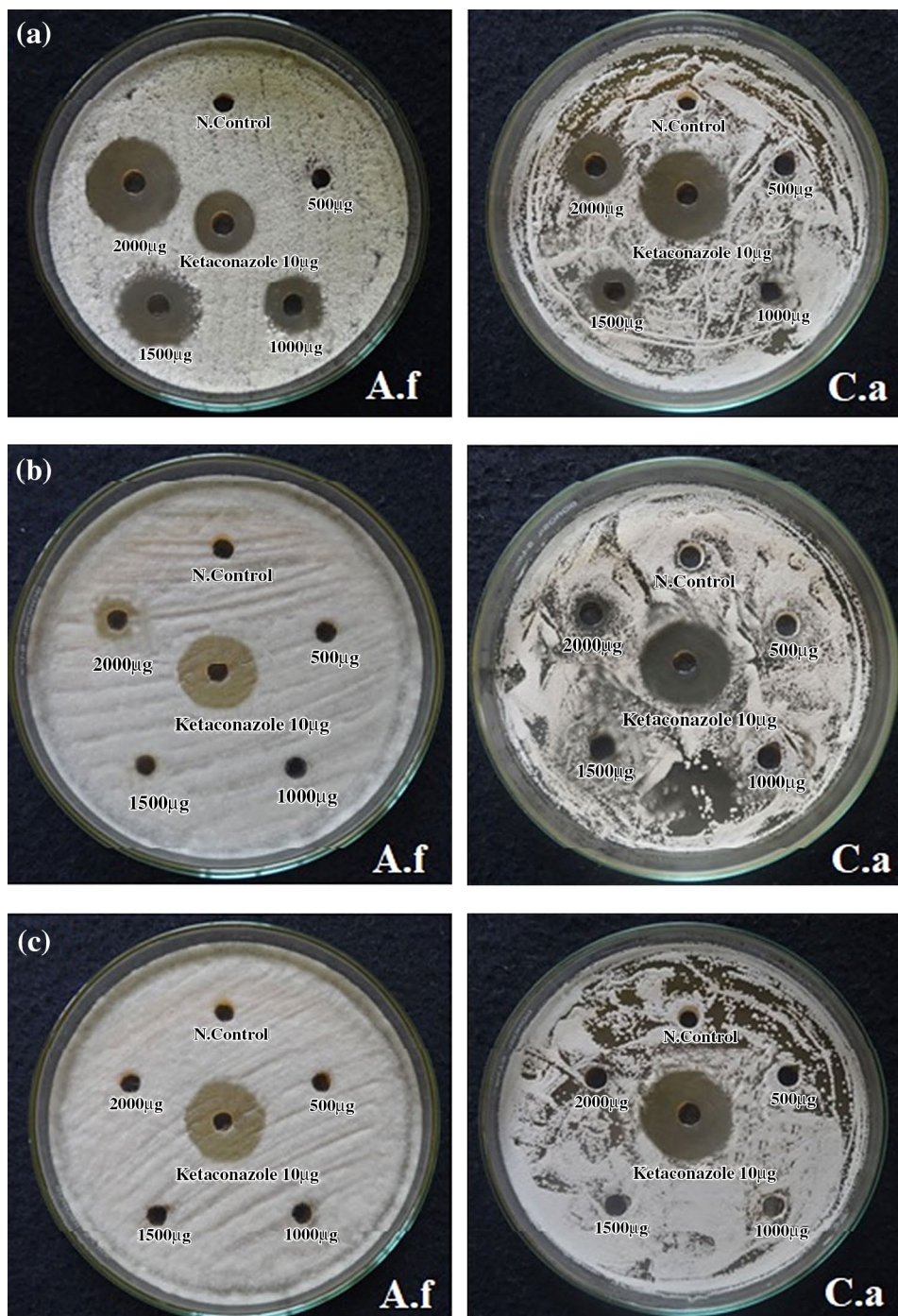
3.9.3 Antioxidant activity

The parent hydrogel and NCHs having antioxidant property contributed by -NH group attached in these compounds [60], which has represented in (Fig. 12a, b). The NCHs have shown higher antioxidant activity than ICD hydrogel due to the presence of AuNPs [61]. The scavenging property of DPPH radical of parent hydrogel (ICD) at various concentration (100, 200, 300, 400 and 500 μg) showed 10, 15, 19, 24 and 29% and NCHs about 36, 42, 58, 60 and 63% for G_1ICD, 38, 44, 60, 62 and 65% for G_2ICD respectively. Similarly, the NO radical scavenging ability results of ICD (3, 5, 10, 15 and 20%), G_1ICD (36, 44, 46, 50 and 59%) and G_2ICD (36, 45, 48, 52 and 61%) with the same concentration of the sample.

Comparatively, NCHs exhibited more antioxidant activity than parent hydrogel (G_2ICD > G_1ICD > ICD), due to the low antibacterial activity of hydrogel leads to

Fig. 11 Antifungal activity of **a** ICD, **b** G$_1$ICD, **c** G$_2$ICD

high antioxidant based on small size and the relatively large surface area of AuNPs resulted in increased antioxidant and declined antibacterial activity [62]. DPPH was a better antioxidant than NO free radical which has represented in the table due to the generation of the nitrite and peroxynitrite anions [63].

3.9.4 Cytotoxicity (MTT assay)

According to the percentages of cell viability above 75% (ISO 10993-5:2009 biological evaluation of medical devices) are considered as a non-toxic compound. The parent hydrogel (ICD) demonstrated the cell viability was found at 100, 97, 92 and 88% at 10, 25, 50, 100 µg/ml which has proved non-toxic nature of hydrogel. However, G$_1$ICD has shown cell viability about 82, 80, 76 and 75% at various
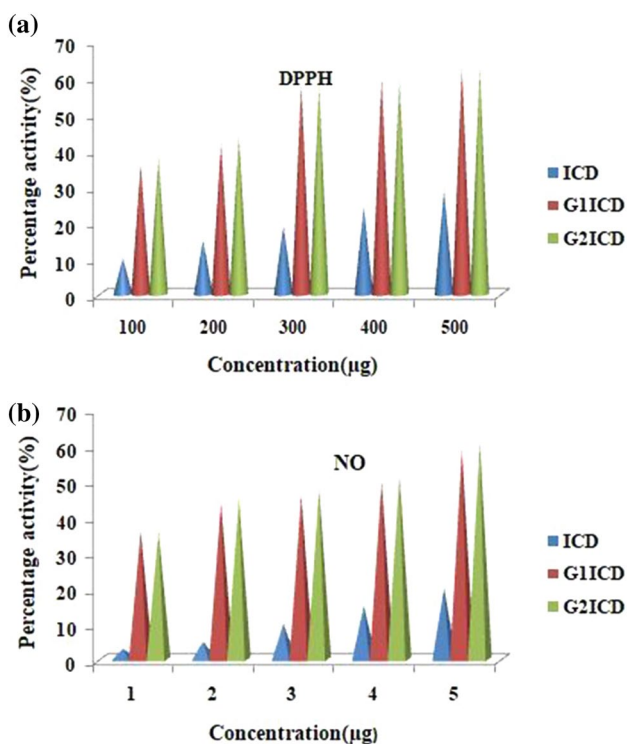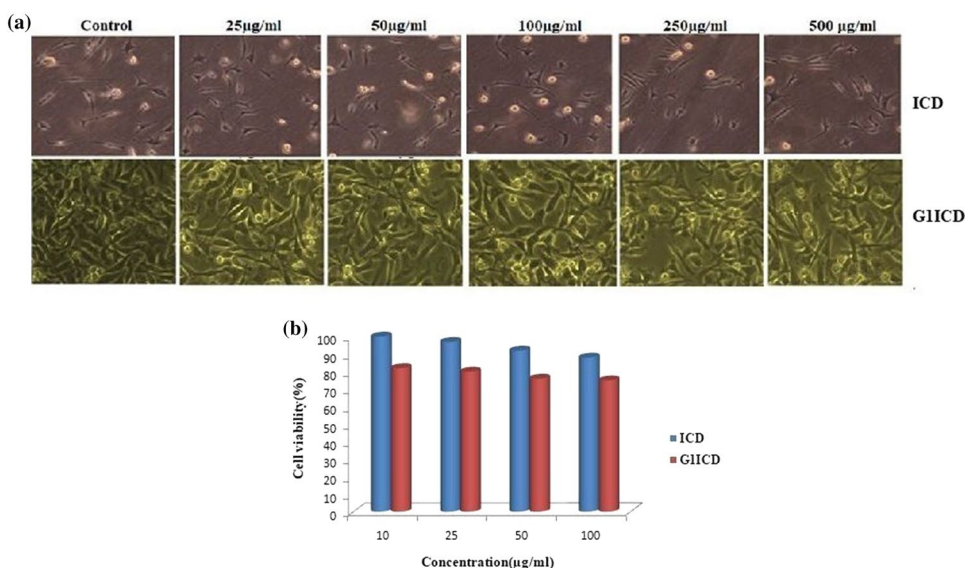
(a)

(b)

Fig. 12 Antioxidant activity **a** DPPH radical, **b** NO radical

Fig. 13 **a** Cytotoxicity effect of ICD and G_1ICD. **b** MTT assay of ICD and G_1ICD

decreasing cell viability which might be possible different mechanisms of discovered AuNPs cellular uptake depending on their size. Importantly, AuNPs induced cell damage is not permanent, meaning that the cells have the ability to recover. On the other hand, the 25 nm AuNPs treatment could generate oxidative stress in a fibroblast cell line [66].

3.9.5 Wound healing activity of hydrogel and NCHs

A major promotion of wound-healing activity was observed for ICD and NCHs in the scratch wound healing model method. The diameter of the wound was monitoring in order to determine the rate of wound closure and wound healing activity. The mean percentage wound closure of parent hydrogel was found to be 0, 34, 55 and 64% and NCH was exhibited 31, 37, 41 and 48% calculated for 0, 24, 48 and 72 h. In particular, fibroblast treatment induced a statistically increases the rate of scratch wound closure (Fig. 14) due to enhanced cell migration. Wound healing properties associated with antioxidant properties, however, to fight free radicals that have the potential to damage biological tissues by disrupting cell membranes.

These free radicals are destructive to molecules in the membrane that contains −C=C bond through oxidation, this happens the ability of the cell to transport substances

concentrations (10, 25, 50, 100 μg/ml). Both parent and NCHs having more than 75% cell viability, therefore both the hydrogel and NCHs suitable material for wound healing application [64]. Comparatively, ICD > G_1ICD, ICD was more cell viability percentage than NCHs which has represented in Fig. 13a and b. ICD hydrogel shown higher nontoxic when indole-3-acetic acid incorporated in hydrogel network [65]. But, the Nanocomposite hydrogel is slightly

across the membrane is affected and moving to its associated poor wound healing process. So, both ICD and NCHs were an excellent antioxidant and cytotoxicity property which leads to better wound healing property [67]. The current application of the treatments efficiently destroyed microbial populations and this lead to better wound healing activity. The primary objective of wound care is to

Fig. 14 Wound healing effect of ICD and G_1ICD
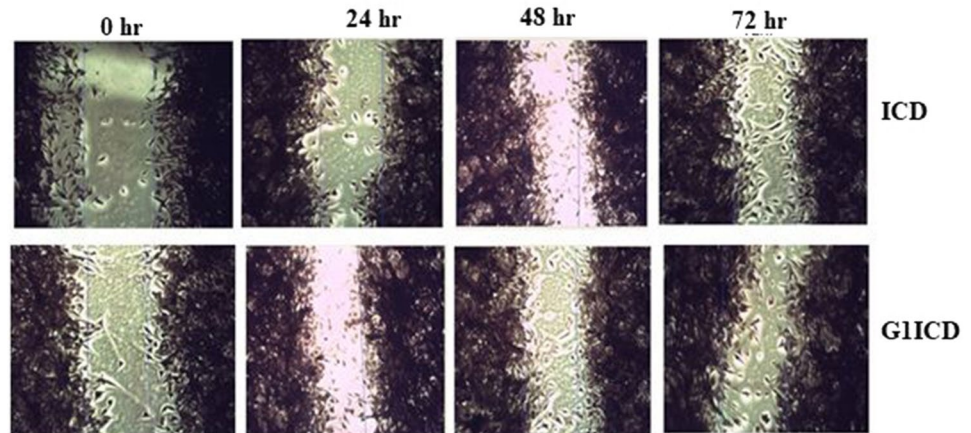
Table 2 Anti-cancer activity of polymeric hydrogel and nanocomposite hydrogels

Concentra-tion (µg/ml)	Cell viability (%)	
	ICD	G_1ICD
25	80	100
50	79	95
100	77	91
250	72	87
500	69	84
Control	100	100

prevent or minimize infection and promote healing. The ability of the hydrogels to decrease the bacterial and fungal load and to inhibit the growth of microbe indicated the wound healing potential [68]. The wound dressing can be enhanced by modification of the physical, chemical, mechanical and hydrogen bonding interaction of indole-3-acetic acid based hydrogels, as well as complexed or cross-linked with other polymers and cross-linking agents. By this approach, it is possible to design the ICD and G_1ICD hydrogels dressings with improved healing properties. The increasing antifungal activity of parent hydrogel (ICD) increase the wound healing activity than NCHs (G_1ICD).

3.9.6 Anticancer activity of hydrogel and NCHs

Table 2 indicates the ICD pure hydrogel-cell viability at various concentration like 25, 50, 100, 250, 500 µg/ml were observed 80, 79, 77, 72 and 69%. Hence, ICD has 69% cancer cell viability at the higher concentration of 500 µg/ml towards non-toxic nature, which has applied for anticancer activity. The cell viability of G_1ICD has observed 100, 95, 91, 87 and 84% with the same concentrations. Table 2 represents anti-cancer cell line viability of ICD and gold nanocomposite hydrogels have observed 69% and 84% at high concentration (500 µg/ml) against the A549 cell line and to fight the cancer cells [69]. The non-toxic effect of gold

nanoparticles in the hydrogel network which might be due to the strong interaction between gold nanoparticles and hydrogel network. Indole-3-acetic acid is among the most valuable, with research having demonstrated their ability to induce cell death in a number of cancer cell lines [70]. Gold nanoparticles incorporated into Indole-3-acetic acid (extracted from plant) based hydrogels, which can then be targeted to various tissues, and more precisely specific targeting of cancer cells.

4 Conclusions

The extraction of indole-3-acetic acid from *Stachytarpheta jamaicensis* has confirmed by ^{1}H NMR and ^{13}C NMR Spectral Studies and HPLC analysis. Indole-3-acetic acid/ DEG hydrogel and their NCHs were prepared by in situ polymerizations of AuNPs. The ICD and its NCHs were fully characterized by FT-IR and UV spectral analysis, TEM, SEM, and EDAX analysis. Thermal stability studied by TGA-DTA analysis. The hydrogel and nanocomposites hydrogels pH-sensitive swelling behavior increased at acidic media and declined at basic media. The order of thermal stability and swelling equilibrium of parent and NCHs were ICD > G_1ICD > G_2ICD. The antifungal activity of the parent hydrogel greater than NCHs using *Aspergillus fumigates* and *Candida albicans* pathogens (ICD > G_1ICD > G_2ICD).

The prepared NCHs have shown excellent antibacterial activity using *S. aureus* and *E. coli* (G_1ICD > G_2ICD), but there is no antibacterial activity observed for ICD. The antioxidant properties of the parent hydrogel and NCHs were in the order of G_2ICD > G_1ICD > ICD using the DPPH and NO radical. Both parent and NCHs were more than 75% cell viability using 3T3 fibroblast cell line, so which has proved non-toxic nature.

Wound healing property could be studied by scratch wound healing assay for 3 days. On comparison increasing

antifungal activity of ICD increasing wound healing activity than NCHs (G_1ICD).

Compliance with ethical standards

Conflict of interest On behalf of all authors, the corresponding author states that there is no conflict of interest.

References

1. Peppas NA (1986) Hydrogels in medicine and pharmacy: fundamentals, vol 1. CRC Press, Boca Raton
2. Brown C, Whitehouse M, Tiekink E, Bushell G (2008) Colloidal metallic gold is not bio-inert. Inflammopharmacology 16:133–137
3. Gaharwar AK, Peppas NA, Khademhosseini A (2014) Nanocomposite hydrogels for biomedical applications. Biotechnol Bioeng 111:441–453
4. Hainfeld JF, Slatkin DN, Focella TM, Smilowitz HM (2006) Gold nanoparticles: a new X-ray contrast agent. Br J Radiol 79:248–253
5. Saha S, Pal A, Pande S, Sarkar S, Panigrahi S, Pal T (2009) Alginate gel-mediated photochemical growth of mono-and bimetallic gold and silver nanoclusters and their application to surface-enhanced Raman scattering. J Phys Chem C 113(18):7553–7560
6. Siiman O, Ledis S (2005) Surface-enhanced Raman scattering (SERS) of random silver or gold particle arrays on aminodextran-coated polystyrene beads. J Raman Spectrosc 36:1125–1133
7. Dotzauer DM, Dai J, Sun L, Bruening ML (2006) Catalytic membranes prepared using layer-by-layer adsorption of polyelectrolyte/metal nanoparticle films in porous supports. Nano Lett 6:2268–2272
8. Murphy CJ, Gole AM, Stone JW, Sisco PN, Alkilany AM, Goldsmith EC, Baxter SC (2008) Gold nanoparticles in biology: beyond toxicity to cellular imaging. Acc Chem Res 41:1721–1730
9. Hernandez-Sierra JF, Ruiz F, Cruz Pena DC, Martinez Gutierrez F, Martinez AE, De Jess Pozos Guillon A, Tapia Perez H, Martinez Castanon G (2008) The antimicrobial sensitivity of *Streptococcus mutans* to nanoparticles of silver, zinc oxide and gold. Nanomed Nanotech Biol Med 4:237–240
10. Eid KAM, Salem HF, Zikry AAF, El-Sayed AFM, Sharaf MA (2011) Antifungal effects of colloidally stabilized gold nanoparticles screening by microplate assay. Nat Sci 9:29–33
11. Ray S, Mohan R, Singh JK, Samantaray MK, Shaikh MM, Panda D, Ghosh P (2007) Anticancer and antimicrobial metallo pharmaceutical agents based on palladium, gold and silver N-heterocyclic carbene complexes. J Am Chem Soc 129:15042–15053
12. Chen X, Schluesener HJ (2008) Nanosilver: a nanoproduct in medical application. Toxicolol Lett 176:1–12
13. Bar-Ilan O, Albrecht RM, Fako VE, Furgeson DY (2009) Toxicity assessments of multisized gold and silver nanoparticles in zebrafish embryos. Small 16:1897–1910
14. Chithrani BD, Ghazani AA, Chan WCW (2006) Determining the size and shape dependence of gold nanoparticle uptake into mammalian cells. Nano Lett 6:662–668
15. Shukla R, Bansal V, Chaudhary M, Basu A, Bhonde RR, Sastry M (2005) Biocompatibility of gold nanoparticles and their endocytotic fate inside the cellular compartment: a microscopic overview. Langmuir 2:10644–10654
16. Travan A, Pelillo C, Donati I, Marsich E, Benincasa M, Scarpa T, Semeraro S, Turco G, Gennaro R, Paoletti S (2009) Non-cytotoxic silver nanoparticle-polysaccharide nanocomposites with antimicrobial activity. Biomacromol 10:1429–1435
17. Elechiguerra JL, Burt J, Morones JR, Camacho Bragado A, Gao X, Lara HH, Yacaman MJ (2005) Interaction of silver nanoparticles with HIV-1. J Nanobiotechnol 3:1–10
18. Prema P, Thangapandiyan S (2013) In-vitro antibacterial activity of gold nanoparticles capped with polysaccharide stabilizing agents. Int J Pharm Pharm Sci 5:310
19. Priyadarshini S, Gopinath V, Priyadharshini NM, Mubarak Ali D, Velusamy P (2013) Biogenic synthesis, characterization of antibacterial silver nanoparticles and its cell cytotoxicity. Colloids Surf B 102:232
20. Puiso J, Jonkuviene D, Macioniene I, Salomskiene J, Jasutiene I, Kondrotas R (2014) Biosynthesis of silver nanoparticles using lingonberry and cranberry juices and their antimicrobial activity. Colloids Surf B 121:214–221
21. Varaprasad K, Vimala K, Ravindra S, Narayana Reddy N, Siva Mohana Reddy G, Mohana Raju K (2012) Biodegradable chitosan hydrogels for in vitro drug release studies of 5-flurouracil an anticancer drug. J Polym Environ 20:573–582
22. Barku VYA, Boye A, Erzah F, Tsamenyi P (2016) In-vitro antioxidant and wound healing properties of combretum dolichopetalum Engl & diels (Combretaceae). J Appl Pharmaceut Sci 6:185–192
23. Jorge MP, Madjarof C, Ruiz ALGT, Fernandes AF, Rodrigues RAF, Sousa IMO, Foglio MA, Carvalho JE (2008) Evaluation of wound healing properties of *Arrabidaea chica* Verlot extract. J Ethnopharmacol 118:361–366
24. Houghton PJ, Hylands PJ, Mensah AY, Hensel A, Deters AM (2005) In vitro tests and ethnopharmacological investigations: wound healing as an example. J Ethnopharmacol 100:100–107
25. Annan K, Houghton PJ (2008) Antibacterial, antioxidant and fibroblast growth stimulation of aqueous extracts of Ficus asperifolia Miq. and Gossypium arboreum L. wound-healing plants of Ghana. J Ethnopharmacol 119:141–144
26. Palluotto F, Carotti A, Casini G, Ferappi M, Rosato A, Vitali C, Campagna F (1999) Synthesis and antibacterial activity of 2-aryl-2, 5-dihydro-3 (3H)-oxo-pyridazino [4,3-*b*] indole-4-carboxylic acids. Farmaco 54:191–194
27. Ryu CK, Lee JY, Park RE, Ma MY, Nho JH (2007) Synthesis and antifungal activity of 1H-indole-4,7-diones. Bioorg Med Chem Lett 17:127–131
28. Gurkok G, Coban T, Suzen S (2009) Melatonin analog new indole hydrazide/hydrazone derivatives with antioxidant behavior: synthesis and structure–activity relationships. J Enz Inhib Med Chem 24:506–515
29. Ates-Alagoz Z, Kus C, Coban T (2005) Synthesis and antioxidant properties of novel benzimidazoles containing substituted indole or 1,1,4,4-tetramethyl-1,2,3,4-tetrahydro-naphthalene fragments. J Enzyme Inhib Med Chem 20:325–331
30. Antosiewicz J, Damiani E, Jassem W, Wozniak M, Orena M, Greci L (1997) Influence of structure on the antioxidant activity of indolinic nitroxide radicals. Free Radic Biol Med 22:249–255
31. Tekiner-Gulbas B, Westwell AD, Suzen S (2013) Oxidative stress in carcinogenesis: new synthetic compounds with dual effects upon free radicals and cancer. Curr Med Chem 20:4451–4459
32. Verm HN, Singh P, Chavan RM (2014) Gold nanoparticle: synthesis and characterization. Vet World 7:72–77
33. Chitra G, Franklin DS, Sudarsan S, Sakthivel M, Guhanathan S (2017) Indole-3-acetic acid/diol based pH-sensitive biological macromolecule for antibacterial, antifungal and antioxidant applications. Intl J Biol Macromol 95:363–375
34. Li H, Qing C, Zhang Y, Zhao Z (2005) Screening for endophytic fungi with antitumour and antifungal activities from chinese medicinal plants world. J Microbiol Biotechnol 21:1515–1519

35. Blois MS (1958) Antioxidant determinations by the use of a stable free radical. Nature 26:1199–1200

36. Naik GN, Pathan AH, Bakale RP, Ligade SG, Gudasi KB (2013) Rare earth complexes of indole-3-acetic acid derived schiff base: synthesis, characterization and plant growth activity. Chem J 3:149–157

37. Michał Szkop and Wiesław Bielawski (2013) A simple method for simultaneous RP-HPLC determination of indolic compounds related to bacterial biosynthesis of indole-3-acetic acid. Antonie Van Leeuwenhoek 103:683–691

38. Franklin DS, Guhanathan S (2015) Influence of chain length of diol on the swelling behavior of citric acid based pH-sensitive polymeric hydrogels: a green approach. J Appl Polym Sci 132:41403

39. Margaret Marie J, Puvanakrishnan R, Nanthini R (2011) Synthesis, characterization and swelling studies of poly (diol citrate-co-diol sebacate) elastomers. Int J Basic Appl Chem Sci 1:46–49

40. Jayaramudu T, Raghavendra GM, Varaprasad K (2016) Preparation and characterization of poly (ethylene glycol) stabilized nanosilver particles by a mechanochemical assisted ball mill process. J Appl Polym Sci 133:43027

41. Bajpai SK, Chand N, Mahendra M (2013) *In situ* formation of silver nanoparticles in poly(methacrylic acid) hydrogel for antibacterial applications. Polym Eng Sci 53:1751–1759

42. Kim JH, Boote BW, Pham JA, Hu J, Byun H (2012) Thermally tunable catalytic and optical properties of gold–hydrogel nanocomposites. Nanotechnology 23:275606–275613

43. Chitra G, Franklin DS, Sudarsan S, Sakthivel M, Guhanathan S (2017) Preparation, antimicrobial and antioxidant evaluation of indole-3-acetic acid-based pH-responsive bio-nanocomposites. Polym Bull 74:3379–3398

44. Haiss W, Thanh NTK, Aveyard J, Fernig DG (2007) Determination of size and concentration of gold nanoparticles from UV-vis spectra. Anal Chem 79:4215–4221

45. Barnes WL, Dereux A, Ebbesen TW (2003) Surface plasmon subwavelength optics. Nature 424:824–830

46. Chen R, Chen Q, Huo D, Ding Y, Yong H, Jiang X (2012) In situ formation of chitosan–gold hybrid hydrogel and its application for drug delivery. Colloids Surf B Biointerfaces 97:132–137

47. Simeonova PP, Opopol N, Luster MI (2007) Nanotechnology–toxicological issues and environmental safety. Springer, Berlin

48. Anuradha J, Abbasi T, Abbasi SA (2010) Rapid and reproducible 'green' synthesis of silver nanoparticles of consistent shape and size using *Azadirachta indica*. Res J Biotechnol 5:75–79

49. Hoak J (2010) A review of the antibacterial effects of silver nanomaterials and potential implications for human health and environment. J Nanoparticle Res 12:1531–1551

50. Chandra Babu A, Prabhakar MN, Suresh Babu A, Mallikarjuna B, Subha MCS, Chowdoji Rao K (2013) Development and characterization of semi-IPN silver nanocomposite hydrogels for antibacterial applications. Int J Carbohydr Chem 2103:1–8

51. Pollini M, Russo M, Licciulli A, Sannino A, Maffezzoli A (2009) Characterization of antibacterial silver-coated yarns. J Mater Sci 20:2361–2366

52. Vimala K, Mohan YM, Varaprasad K, Reddy NN, Ravindra S, Naidu NS, Raju KM (2011) Fabrication of curcumin encapsulated Chitosan-PVA Silver nanocomposite films for improved antimicrobial activity. J Biomater Nanobiotechnol 2:55–64

53. Ma YQ, Yi JZ, Zhang LM (2009) A facile approach to incorporate silver nanoparticles into dextran-based hydrogels for antibacterial and catalytical application. J Macromol Sci Part A Pure Appl Chem 6:643–648

54. Lee KH, Rah SC, Kim SG (2008) Formation of monodisperse silver nanoparticles in poly (vinylpyrrolidone) matrix using spray pyrolysis. J Sol-Gel Sci Tech 45:187–193

55. Zhou Y, Kong Y, Kundu S, Cirillo JD, Liang H (2012) Antibacterial activities of gold and silver nanoparticles against *Escherichia coli* and Bacillus Calmette-Guérin. J Nanobiotechnol 10:19

56. Zhang Y, Peng H, Huang W, Zhou Y, Yan D (2008) Facile preparation and characterization of highly antimicrobial colloid Ag or Au nanoparticles. J Colloid Interface Sci 325:371–376

57. Sondi I, Salopek-Sondi B (2004) Silver nanoparticles as antimicrobial agent: a case study on *E. coli* as a model for Gram-negative bacteria. J Colloid Interface Sci 275:177–182

58. Tokeer Ahmad A, Wani IA, Lone IH, Ganguly A, Manzoor N, Ahmad A, Ahmed J, Al-Shihri AS (2013) Antifungal activity of gold nanoparticles prepared by solvothermal method. Mater Res Bull 48:12–20

59. Liao RS, Rennie RP, Talbot JA (1999) Assessment of the effect of amphotericin B on the vitality of *Candida albicans*. Antimicrob Agents Chemother 43:1034–1041

60. Naik N, Kumar HV, Harini ST (2011) Synthesis and antioxidant evaluation of novel indole-3-acetic acid analogues. Eur J Chem 2:337–341

61. Chen Q, Jiang H, Ye H, Li J, Huang J (2014) Preparation of antibacterial and antioxidant activities of silver/chitosan composites. J Carbohydr Chem 33:298–312

62. Devashri Sahu GM, Kannan MT, Vijayaraghavan R (2016) In vitro cytotoxicity of nanoparticles: a comparison between particle size and cell type. J Nanosci 2016:1–9

63. Abdel-Aziz MS, Shaheen MS, El-Nekeety AA, Abdel-Wahhab MA (2013) Antioxidant and antibacterial activity of silver nanoparticles biosynthesized using *Chenopodium murale* leaf extract. J Saudi Chem Soc 18:356–364

64. Chitra G, Franklin DS, Guhanathan S (2017) Indole-3-acetic acid based tunable hydrogels for antibacterial, antifungal and antioxidant applications. Int J Macromol Sci Pure Appl Chem Part A 54:151–163

65. De Melo MP, De Lima MP, Pithon Curi TC, Curi R (2004) The mechanism of indole acetic acid cytotoxicity. Toxicol Lett 148:103–111

66. Chithrani BD, Chan WCW (2007) Elucidating the mechanism of cellular uptake and removal of protein-coated gold nanoparticles of different sizes and shapes. Nano Lett 7:1542–1550

67. Suntar I, Kupeli AE, Nahar L, Satyajit D, Sarker SD (2012) Wound healing and antioxidant properties: do they coexist in plants. Free Radic Antioxid 2:1–7

68. Okoli CO, Akah PA, Okoli AS (2007) Potentials of leaves of *Aspilia africana* (Compositae) in wound care: an experimental evaluation. BMC Complement Altern Med 7:24

69. Nam J, Won N, Jin H, Chung H, Kim S (2009) pH-induced aggregation of gold nanoparticles for photothermal cancer therapy. J Am Chem Soc 131:13639–13645

70. El Sayed MT et al (2015) Indoles as anticancer agents. Adv Mod Oncol Res 1:20–25